RESEARCH ARTICLE SUMMARY

NEURODEVELOPMENT

Retinal waves prime visual motion detection by simulating future optic flow

Xinxin Ge†, Kathy Zhang†, Alexandra Gribizis, Ali S. Hamodi, Aude Martinez Sabino, Michael C. Crair*

INTRODUCTION: Fundamental circuit features of the mouse visual system emerge before the onset of vision, allowing the mouse to perceive objects and detect visual motion immediately upon eye opening. How the mouse visual system achieves self-organization by the time of eye opening without structured external sensory input is not well understood. In the absence of sensory drive, the developing retina generates spontaneous activity in the form of propagating waves. Past work has shown that spontaneous retinal waves provide the correlated activity necessary to refine the development of gross topographic maps in downstream visual areas, such as retinotopy and eye-specific segregation, but it is unclear whether waves also convey information that instructs the development of higher-order visual response properties, such as direction selectivity, at eye opening.

RATIONALE: Spontaneous retinal waves exhibit stereotyped changing spatiotemporal patterns throughout development. To characterize the spatiotemporal properties of waves during development, we used one-photon wide-field calcium imaging of retinal axons projecting to the superior colliculus in awake neonatal mice. We identified a consistent propagation bias that occurred during a transient developmental window shortly before eye opening. Using quantitative analysis, we investigated whether the directionally biased retinal waves conveyed ethological information relevant to future visual inputs. To understand the origin of directional retinal waves, we used pharmacological, optogenetic, and genetic strategies to identify the retinal circuitry underlying the propagation bias. Finally, to evaluate the role of directional retinal waves in visual system development, we used pharmacological and genetic strategies to chronically manipulate wave directionality and used two-photon calcium imaging to measure responses to visual motion in the midbrain superior colliculus immediately after eye opening.

RESULTS: We found that spontaneous retinal waves in mice exhibit a distinct propagation bias in the temporal-to-nasal direction during a transient window of development (postnatal day 8 to day 11). The spatial geometry of directional wave flow aligns strongly with the optic flow pattern generated by forward self-motion, a dominant natural optic flow pattern after eye opening. We identified an intrinsic asymmetry in the retinal circuit that enforced the wave propagation bias involving the same circuit elements necessary for motion detection in the adult retina, specifically asymmetric inhibition from starburst amacrine cells through γ-aminobutyric acid type A ($GABA_A$) receptors. Finally, manipulation of directional retinal waves, through either the chronic delivery of gabazine to block GABAergic inhibition or the starburst amacrine cell–specific mutation of the *FRMD7* gene, impaired the development of responses to visual motion in superior colliculus neurons downstream of the retina.

CONCLUSION: Our results show that spontaneous activity in the developing retina prior to vision onset is structured to convey essential information for the development of visual response properties before the onset of visual experience. Spontaneous retinal waves simulate future optic flow patterns produced by forward motion through space, due to an asymmetric retinal circuit that has an evolutionarily conserved link with motion detection circuitry in the mature retina. Furthermore, the ethologically relevant information relayed by directional retinal waves enhances the development of higher-order visual function in the downstream visual system prior to eye opening. These findings provide insight into the activity-dependent mechanisms that regulate the self-organization of brain circuits before sensory experience begins. ■

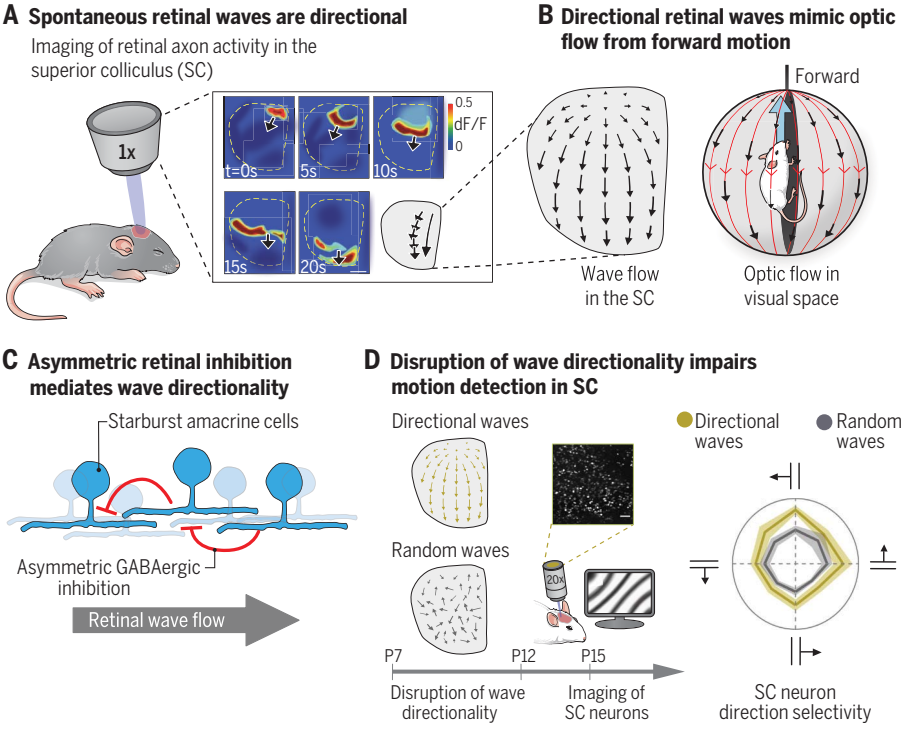

Origin and function of directional retinal waves. (**A**) Imaging of retinal axon activity reveals a propagation bias in spontaneous retinal waves (scale bar, 500 μm). (**B**) Cartoon depiction of wave flow vectors projected onto visual space. Vectors (black arrows) align with the optic flow pattern (red arrows) generated by forward self-motion. (**C**) Asymmetric GABAergic inhibition in the retina mediates wave directionality. (**D**) Developmental manipulation of wave directionality disrupts direction-selective responses in downstream superior colliculus neurons at eye opening.

Department of Neuroscience, Yale University School of Medicine, New Haven, CT 06510, USA.
***Corresponding author. Email: michael.crair@yale.edu**
†These authors contributed equally to this work.
Cite this article as X. Ge *et al.*, *Science* 373, eabd0830 (2021). DOI: 10.1126/science.abd0830

RESEARCH ARTICLE

NEURODEVELOPMENT

Retinal waves prime visual motion detection by simulating future optic flow

Xinxin Ge†‡, Kathy Zhang†, Alexandra Gribizis§, Ali S. Hamodi, Aude Martinez Sabino¶, Michael C. Crair*

The ability to perceive and respond to environmental stimuli emerges in the absence of sensory experience. Spontaneous retinal activity prior to eye opening guides the refinement of retinotopy and eye-specific segregation in mammals, but its role in the development of higher-order visual response properties remains unclear. Here, we describe a transient window in neonatal mouse development during which the spatial propagation of spontaneous retinal waves resembles the optic flow pattern generated by forward self-motion. We show that wave directionality requires the same circuit components that form the adult direction-selective retinal circuit and that chronic disruption of wave directionality alters the development of direction-selective responses of superior colliculus neurons. These data demonstrate how the developing visual system patterns spontaneous activity to simulate ethologically relevant features of the external world and thereby instruct self-organization.

Essential functions of the mammalian visual system, including the ability to locate objects and detect motion, are present even at the first onset of vision (*1*–*7*). How the visual system organizes its functional maturation before the start of sensory experience remains unclear. Prior to vision, spontaneous retinal activity occurs in the form of propagating waves that spread throughout the ascending visual system (*8*–*10*). Spontaneous retinal waves correlate the activity of neighboring cells in the retina and, through a Hebb-based mechanism, are critical for the development of visual maps (such as retinotopy and eye-specific segregation) that reflect near-neighbor relations in visual space (*1*, *2*, *11*–*21*). Whether and how the spatiotemporal pattern of spontaneous retinal waves conveys additional information beyond the gross correlations between topographically neighboring cells and contributes to the development of higher-order visual response properties remains unclear.

Spontaneous retinal waves in mice are divided into three stages according to their requisite mode of interneuronal communication (fig. S1A) (*22*). The spatiotemporal pattern of waves differs across these stages (*10*, *23*, *24*), but relatively little is known about whether or which of these spatiotemporal features might be relevant for visual system development. Previous studies have shown that retinal waves exhibit an early bias in propagation direction of unknown origin and function (*9*, *10*, *18*). In amphibian larvae, whose development takes place largely externally and in the presence of visual stimuli capable of driving retinal activity, the direction of visual optic flow as the animal moves through space instructs visual system development (*25*). We sought to examine whether the directional propagation bias of spontaneous retinal waves prior to eye opening might also convey critical information for the functional maturation of the visual system in mammals.

Department of Neuroscience, Kavli Institute for Neuroscience, Yale University School of Medicine, New Haven, CT 06510, USA. *Corresponding author. Email: michael.crair@yale.edu
†These authors contributed equally to this work. ‡Present address: Department of Physiology, University of California, San Francisco, CA 94158, USA. §Present address: Department of Functional Architecture and Development of Cerebral Cortex, Max Planck Florida Institute for Neuroscience, Jupiter, FL 33458, USA. ¶Present address: Bioengineering Department, University of Technology of Compiègne, 60200 Compiègne, France.

Directional retinal waves resemble future optic flow

To determine the developmental time course of the directional bias in retinal waves, we examined the spontaneous activity of retinal ganglion cells in young mice at multiple ages throughout development in vivo. Spontaneous retinal activity was imaged in topographically mapped retinal ganglion cell axon arbors in the superior colliculus (Fig. 1A). To gain full access to retinal activity, we used Emx1-Cre; Tra2β$^{f/f}$ mice (cortexless mice) (*26*), which have a completely exposed superior colliculus due to suppressed cortical neurogenesis. Retinal ganglion cells were labeled with the genetically encoded calcium indicator GCaMP6s by intraocular injections of AAV2/1-hSyn-GCaMP6s virus at postnatal day 0 to 1 (P0–P1) for calcium imaging of activity in retinal axon arbors in the superior colliculus at later ages (Fig. 1A). Spontaneous retinal activity was observed in all age groups between P3 and P29 in head-fixed, awake mice (movie S1).

During the first two postnatal weeks, wave directionality changed together with other spatiotemporal properties of waves, such as wave interval, duration, size, and propagation distance (fig. S1). In retinal coordinates, used throughout for data presentation and description, retinal waves exhibited a temporal-to-nasal directional bias, corresponding to forward-to-backward motion in visual space. The wave directional bias spanned the end of stage 2 (P8–P9) and persisted into stage 3 (P10–P11) (Fig. 1C and fig. S1F), even though waves at P8–P9 and P10–P11 differed in other spatiotemporal properties (Fig. 1B, fig. S1, B to E, and table S1). To exclude the possibility that the wave directional bias was due to the loss of cortex in Emx1-Cre; Tra2β$^{f/f}$ mice, we also examined retinal activity in mice with an intact cortex. A similar pattern of wave directionality was observed in mice with an intact cortex and in Emx1-Cre; Tra2β$^{f/f}$ (cortexless) mice with a restricted field of view to resemble cortex-intact mice (fig. S2 and table S1). These results reveal the presence of a developmentally transient temporal-to-nasal bias in wave propagation direction that spanned both stage 2 and stage 3 waves.

To examine whether locations across the superior colliculus experienced a consistent directional bias, we quantified the average wave propagation across each pixel separately. The pixel-based directionality analysis confirmed the temporal-to-nasal wave-based analysis across development (fig. S3). However, the pixel-based flow patterns were inhomogeneous and stereotypically deviated from the dominant temporal-to-nasal wave direction, depending on location in the superior colliculus (Fig. 1D and fig. S4A). We investigated the relationship between this stereotyped wave flow pattern and optic flow by first measuring retinotopy in the superior colliculus of cortexless mice after eye opening (~P21) (fig. S4B). We then compared the wave flow patterns with translatory or rotatory optic flow fields. To quantify the alignment between wave flow and translatory or rotatory optic flow fields, we calculated a concordance index (*27*) as the percentage of pixels with wave flow within 10° of local optic flow. We found that wave flow vectors were significantly better aligned with a translatory optic flow field than with a rotary optic flow field (Fig. 1, E and F). The translatory optic flow alignment was best fit with a center of expansion in the temporal retina, consistent with the flow patterns produced by forward self-motion through space (fig. S5). These results demonstrate that spontaneous retinal waves prior to eye opening resemble forward translatory optic flow, the dominant future optic flow pattern received by animals as they move through space after eye opening.

Asymmetric GABAergic inhibition mediates wave directionality

To investigate whether directional retinal waves affect visual system development, we

sought to first understand the origin of wave directionality. We considered two nonexclusive mechanisms for wave directionality (Fig. 2A). The first is an intrinsic propagation bias: an asymmetric retinal circuit that intrinsically favors wave propagation in the temporal-to-nasal direction. The second potential mechanism is an initiation bias: a tendency for waves to initiate at the temporal edge of the retina that could cause an overall temporal-to-nasal directionality as waves travel away from the temporal edge.

We first examined the possibility of a propagation bias mechanism by assessing the directionality of waves initiated from the nasal part

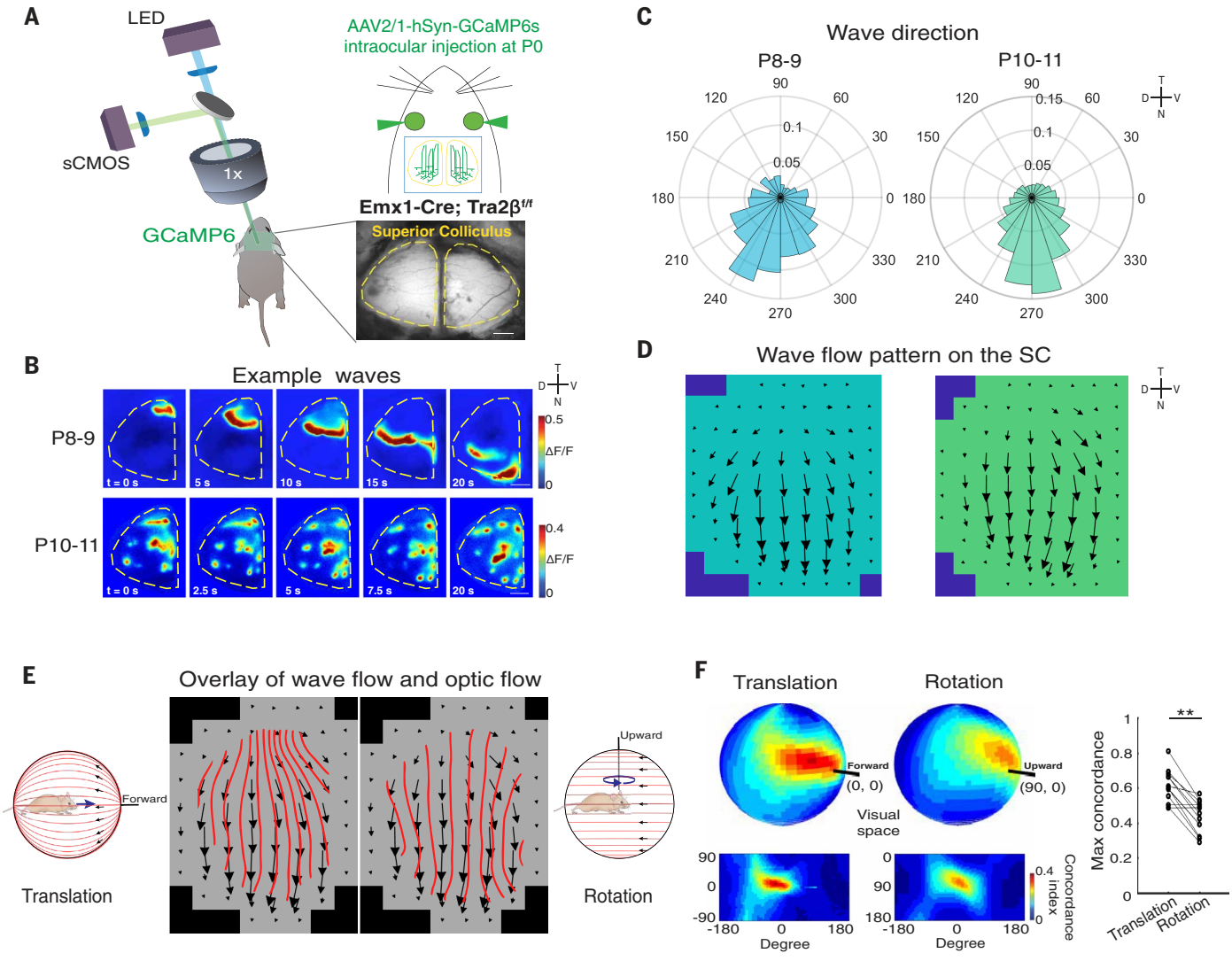

Fig. 1. Spontaneous retinal waves are directional and resemble translatory optic flow during a transient developmental window. (**A**) Schematic showing the wide-field single-photon microscopy used to perform Ca^{2+} imaging of retinal ganglion cell axon activity in the superior colliculus (SC). GCaMP6s expression in retinal ganglion cells was achieved by intraocular injections of AAV2/1-hSyn-GCaMP6s at P0 in Emx1-Cre; $Tra2\beta^{f/f}$ mice. A cranial window above the SC was surgically prepared before imaging. Mice were unanesthetized and head-fixed during the imaging. Scale bar, 500 μm. (**B**) ΔF/F montages of example waves at P8–P9 (top) and P10–P11 (bottom). (**C**) Frequency distributions of propagation directions for all waves at P8–P9 [n = 5 hemispheres, 831 waves, total circular variance (CV) = 0.6087] and at P10–P11 (n = 8 hemispheres, 7937 waves, total CV = 0.5611). Inset at right: Directions T, N, D, and V correspond to temporal, nasal, dorsal, and ventral in the retina unless otherwise stated. (**D**) Averaged pixel-based wave flow fields on the SC at P8–P9 (left) and at P10–P11 (right). (**E**) Left: Optic flow pattern produced by an animal's forward translation through space, and an overlay between average wave flow (black arrows) and the translatory optic flow that best matched with wave flow (red lines) on the left SC. Right: Optic flow induced by an animal's rotation in space, and an overlay between average wave flow and rotatory optic flow that best matched with wave flow on the SC. Wave flow was averaged from all recordings at P8–P11 (n = 13 hemispheres). Optic flow fields were generated from retinotopic maps in the SC (see supplementary materials for details). Forward and upward indicate directions in visual space. (**F**) Concordance index between wave and translatory or rotatory optic flow as a function of the axis of the animal's translation or rotation. All possible axes of translation or rotation were tested. Concordance index is the percentage of pixels on the SC that have the same direction (<10° difference) as the local optic flow. Top: Spherical maps of average concordance index (n = 13 hemispheres) between wave and translatory (top left) and rotatory (top right) optic flow in global visual space. The best match between wave flow and optic flow due to translation deviated slightly from forward motion (10° elevation and 15° azimuth). Bottom: Flattened concordance maps. Black bars indicate the forward and upward directions in visual space. Right: Maximum concordance index between individual wave flow fields and translatory optic flow was much higher than rotatory optic flow (translatory, 0.611 ± 0.026; rotatory, 0.438 ± 0.025; n = 13 hemispheres; $^{**}P$ = 0.0012, Wilcoxon signed-rank test). $^{*}P < 0.05$, $^{**}P < 0.01$, $^{***}P < 0.001$. Data are means ± SEM.

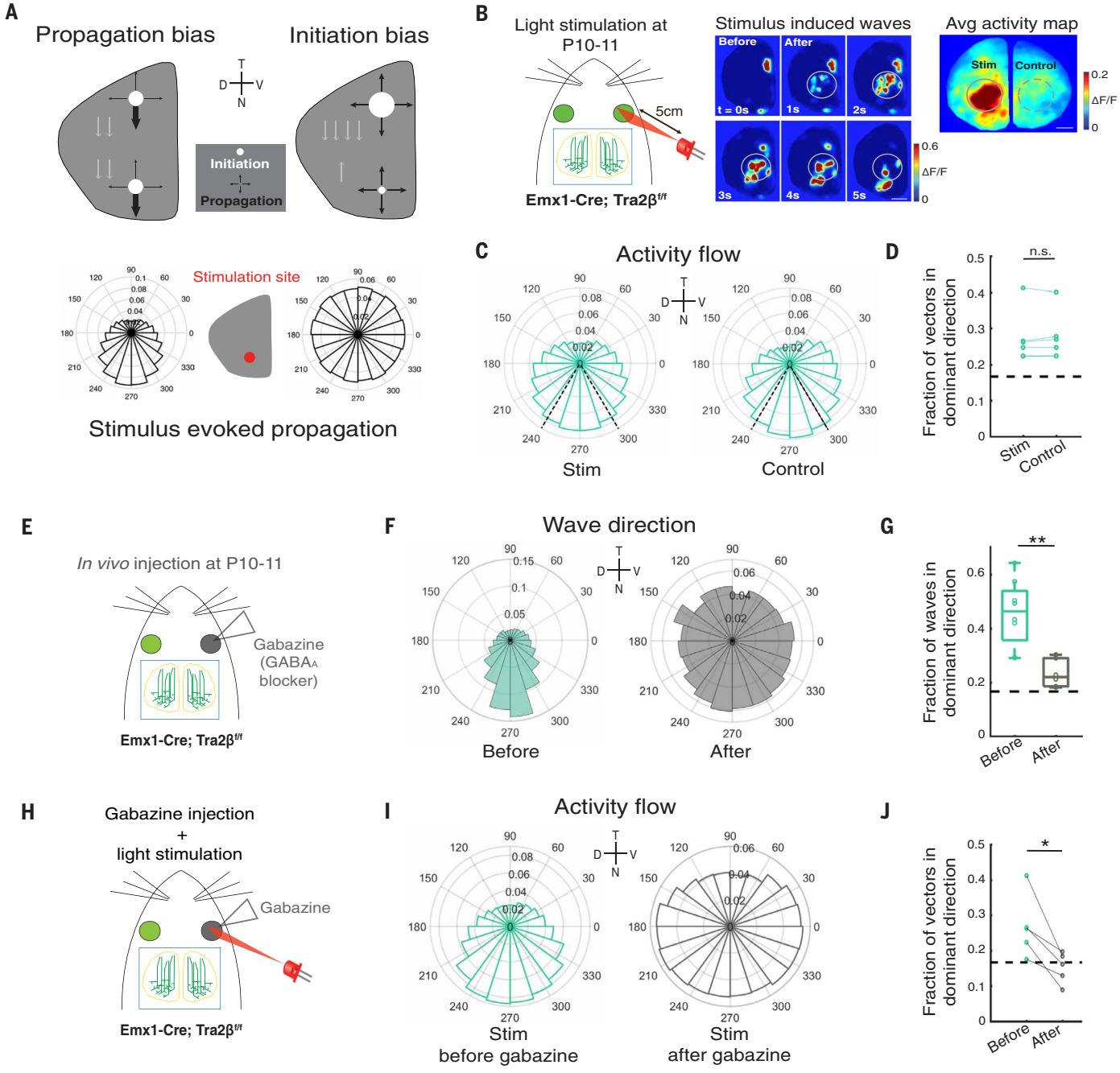

Fig. 2. Wave directionality requires a propagation bias mediated by asymmetric GABAergic inhibition. (**A**) Possible mechanisms of wave directionality. Top left: Wave bias may be generated by a propagation bias in the retinal circuitry that favors wave propagation in the temporal-to-nasal direction. Top right: Biased initiation in the temporal retina can induce wave directional bias. White circles, likelihood of initiation; black arrows, likelihood of propagation in certain directions. Bottom: Hypothetical propagation directions for waves stimulated in the nasal retina for the two proposed mechanisms. (**B**) Left: At P10–P11, light stimulation was performed in Emx1-Cre; Tra2β$^{f/f}$ mice that had received intraocular injections of AAV2/1-hSyn-GCaMP6s at P0–P1. The 615-nm LED strobe was placed ~5 cm away from the stimulated eye and was oriented toward the nasal retina. Light stimuli had a duration of 500 ms and were repeated every 30 s. Center: Example montages of waves induced by light stimulation at P10–P11. Right: Averaged activity 0 to 10 s after each stimulation in the same example animal. Solid circles (stim, surrounding the stimulation site) and dashed circles [control, mirrored region of interest (ROI) in the opposite hemisphere] indicate the ROIs that were selected for the analyses of wave propagation directions. (**C**) Pooled pixel-based activity flow directions within stim (left) and control (right) ROIs 0 to 10 s after each stimulation (n = 5 animals; stim, total CV = 0.680; control, total CV = 0.682). Dashed black lines indicate the 60° around the dominant direction that was used for further analyses. (**D**) Proportion of pixel-based activity flow vectors within 60° around the dominant direction. Each data point represents one hemisphere; data points from the same animal were paired. Dashed black line, fraction in the dominant direction if wave propagation directions are random (stim, 0.282 ± 0.033; control, 0.284 ± 0.030; P = 0.625, Wilcoxon signed-rank test). (**E**) Gabazine (50 μM) was applied in vivo at P10 in Emx1-Cre; Tra2β$^{f/f}$ mice that received intraocular injections of AAV2/1-hSyn-GCaMP6s at P0–P1. (**F**) Frequency distributions of wave propagation directions in animals without gabazine injection (before, n = 8 hemispheres, total CV = 0.561) or after gabazine injection

(after, n = 6 hemispheres, total CV = 0.931) at P10. (**G**) Gabazine reduced the proportion of waves propagating within 60° of the dominant temporal-to-nasal direction (control, 0.456 ± 0.044; gabazine, 0.234 ± 0.021; $^{**}P$ = 0.003, Wilcoxon rank sum test). (**H**) Light stimuli were applied in Emx1-Cre; Tra2β$^{f/f}$ mice before and after gabazine injection to the eye, following the same protocol described in (A). (**I**) Pixel-based activity flow directions within stim ROIs 0 to 10 s after each stimulation before (n = 5 animals, total CV = 0.682) and after gabazine injection (n = 5 animals, total CV = 0.938). (**J**) Gabazine injections reduced the proportion of pixel-based activity flow vectors within 60° surrounding the dominant direction. Data points from the same hemisphere were paired (before, 0.267 ± 0.040; after, 0.152 ± 0.020; $^{*}P$ = 0.031, one-tailed Wilcoxon signed-rank test). All boxplots report medians with the 75% confidence interval unless otherwise noted.

of the retina at P10–P11 (Fig. 2A). To control the site of wave initiation, we made use of exogenous stimuli. Starting around P9, photoreceptors are weakly but functionally integrated into the retinal circuit (*28*–*31*), which enabled us to evoke waves using focal light stimuli (Fig. 2B and movie S2). Waves stimulated in the nasal retina at P10–P11 exhibited the same temporal-to-nasal bias as spontaneous retinal waves (Fig. 2, C and D), suggesting an inherent anisotropy in retinal circuitry that favors retinal wave propagation in the temporal-to-nasal direction at this age. Consistent with P10–P11, P8–P9 waves initiated in the nasal retina exhibited the same temporal-to-nasal bias (fig. S6, A to C). To ensure that the propagation bias was not an artifact of stimulation, we examined waves initiated in the nasal retina at P6–P7 when spontaneous retinal waves are not biased in the temporal-to-nasal direction. At this age, waves were initiated by optogenetic stimulation of starburst amacrine cells, interneurons that are responsible for stage 2 wave initiation and propagation (fig. S6A and movie S3). In contrast to P8–P9 and P10–P11, waves initiated in the nasal retina at P6–P7 were not biased in the temporal-to-nasal direction (fig. S6, B and C). We next quantified the distribution of wave initiation locations at P8–P9 and P10–P11. Although waves were equally likely to initiate from any location in the retina at P10–P11, there was an initiation bias at P8–P9 (fig. S6D). The initiation bias at P8–P9 could be due to an extra source of excitatory drive in the temporal retina at this age, or could be a consequence of the slow afterhyperpolarizations in the recurrent network of starburst amacrine cells that entrains an initiation zone (*22*, *32*–*34*). Regardless, neonatal mice at both P8–P9 and P10–P11 displayed a consistent retinal circuit propagation bias, which suggests a generic role of intrinsic propagation anisotropy in mediating retinal wave directionality that is absent at P6–P7.

We next investigated the origin of the propagation anisotropy described above. In the adult mouse retina, direction selectivity in retinal ganglion cells is achieved through asymmetric γ-aminobutyric acid–mediated (GABAergic) inhibition (*35*, *36*). We reasoned that asymmetric circuit wiring might also be present during development and provide imbalanced inhibition to waves propagating in different directions to generate the observed propagation anisotropy. To determine whether asymmetric inhibition is involved in wave directionality, we examined wave directionality after the application of inhibitory antagonists to the retina in vivo at P10 (Fig. 2E). Application of gabazine, a $GABA_A$ receptor ($GABA_AR$) antagonist, significantly reduced the wave directional bias (Fig. 2, F and G, and movie S4), whereas applications of TPMPA, a $GABA_C$ receptor ($GABA_CR$) antagonist, or strychnine, an antagonist of glycine, had little effect (fig. S7, A to C). As a result of disrupted wave directionality, the concordance between translatory optic flow and wave flow was significantly reduced after gabazine injection (fig. S7H). No other spatiotemporal feature was significantly altered by gabazine application, suggesting the specificity of $GABA_ARs$ at this age in mediating wave directionality (fig. S7, D to G, and table S1). We further examined the directionality of exogenously stimulated waves after retinal application of gabazine (Fig. 2H). Consistent with the significant reduction of directional bias in spontaneous waves, stimulated waves were similarly disrupted after gabazine application (Fig. 2, I and J). These data demonstrate that asymmetric inhibition mediated by retinal $GABA_ARs$ is crucial for wave directionality.

Wave directionality requires starburst amacrine cells

We next sought to identify the underlying cellular components that produce the asymmetric inhibition necessary for wave directionality. Starburst amacrine cells are known to confer motion direction-selective responses on direction-selective ganglion cells in the adult mouse retina (*35*, *37*). This property suggests starburst amacrine cells as a candidate for providing asymmetric inhibition in wave propagation. However, in the developing retina, starburst amacrine cells are only thought to generate stage-2 retinal waves via their recurrent excitatory network (*33*), and little is known about the role of inhibition from starburst amacrine cells in wave propagation. To examine the role of starburst amacrine cells in directional waves, we selectively ablated starburst amacrine cells through daily retinal application of diphtheria toxin (DT) from P5 to P7 in ChAT-Cre; LSL-DTR mice, which specifically express DT receptors in starburst amacrine cells (Fig. 3, A and B), and examined wave directionality at P10. Retinal waves in P10 starburst amacrine cell–ablated animals maintained a normal peak wave area and propagation distance relative to controls (fig. S8, B to E, table S1, and movie S5) but had significantly disrupted wave directionality (Fig. 3, D and E). Wave directionality in starburst amacrine cell–ablated animals was not further altered after gabazine injection (fig. S8A), consistent with $GABA_AR$-dependent wave directionality acting through starburst amacrine cells. These results reveal that generation of the temporal-to-nasal wave directional bias observed at P10 requires starburst amacrine cells.

To further identify the features of starburst amacrine cells crucial for wave directionality, we examined retinal waves in transgenic animals that have a starburst amacrine cell–specific mutation of the *FRMD7* gene (*38*, *39*). In the adult retina, mutation of *FRMD7* abolishes temporal and nasal retinal ganglion cell direction selectivity by eliminating the asymmetry of inhibition from starburst amacrine cells onto temporal- or nasal-preferring direction-selective ganglion cells (*38*). During development, spontaneous retinal waves in FRMD7^{tm} mice displayed a significant disruption in wave directionality similar to that observed in starburst amacrine cell–ablated animals (Fig. 3, F and G). The disruption in wave directionality in FRMD7^{tm} mice was not further altered by gabazine (fig. S6F), and other wave properties remained unchanged (fig. S6, G to J, table S1, and movie S5). These results show that asymmetric inhibition from starburst amacrine cells, which confer direction selectivity in the adult retina, is also necessary for mediating temporal-to-nasal wave directionality during development. Taken together with the finding that gabazine blocks wave directionality, our data suggest that asymmetric $GABA_AR$-mediated inhibition by starburst amacrine cells is necessary for the transient temporal-to-nasal directional bias in spontaneous retinal waves during development.

Because starburst amacrine cells in the adult retina provide asymmetric inhibition to downstream direction-selective ganglion cells as well as to neighboring starburst amacrine cells or other amacrine cells (*27*, *37*, *40*, *41*), it remains unclear which asymmetric inhibitory connection mediates wave directionality. To determine whether starburst amacrine cells modulate wave directionality by providing asymmetric inhibition onto direction-selective ganglion cells, we examined wave directionality in two different subtypes of direction-selective ganglion cells: Cdh6-positive ganglion cells that receive asymmetric inhibition from starburst amacrine cells along the dorsal-ventral axis

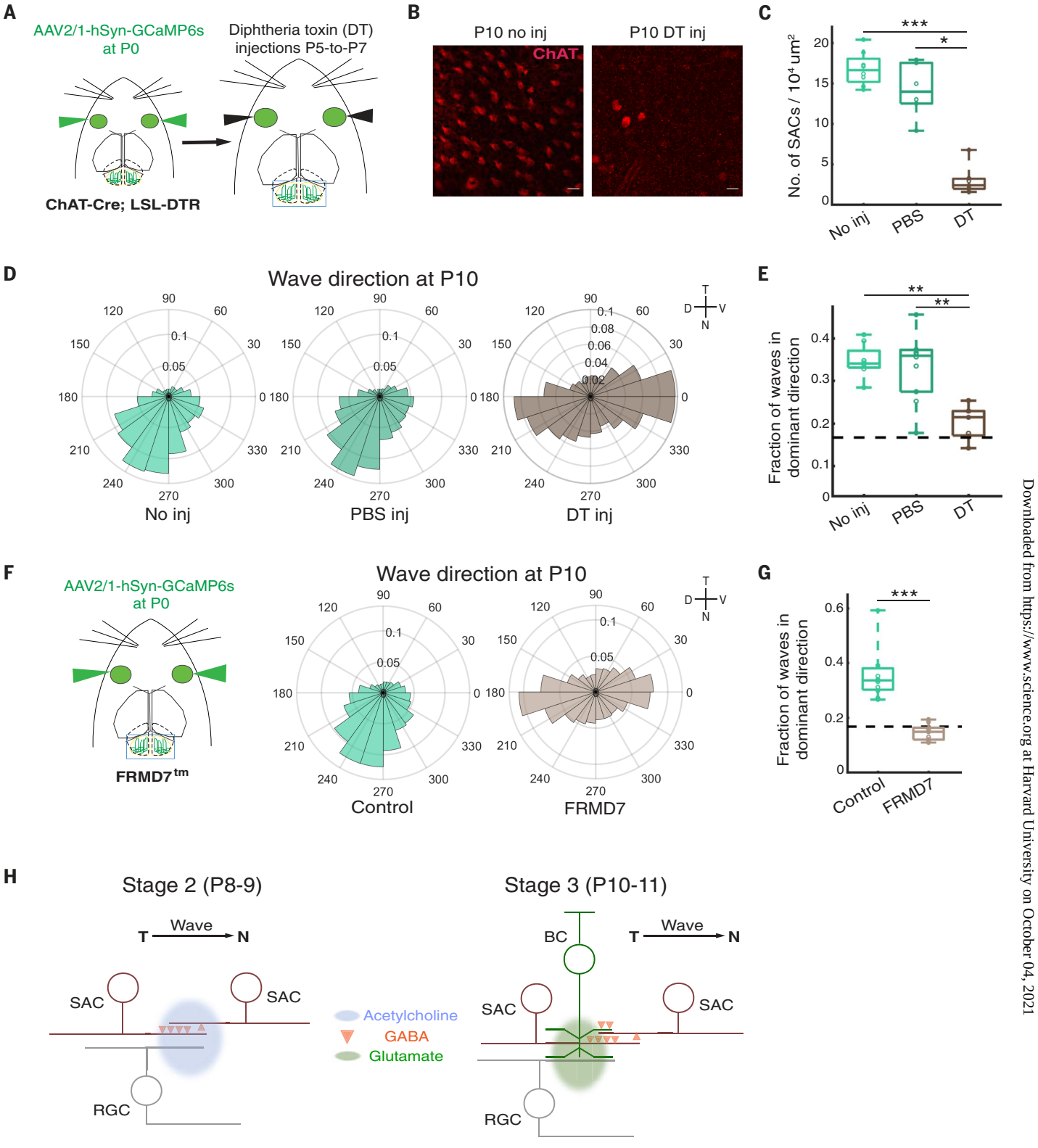

Fig. 3. Starburst amacrine cells (SACs) mediate wave directionality. (**A**) AAV2/1-hSyn-GCaMP6s was intraocularly injected in ChAT-Cre; LSL-DTR mouse pups at P0. Intraocular injections of diphtheria toxin (DT, 0.8 ng/μl, or PBS as controls) were performed every 24 hours between P5 and P7. (**B**) Immunostaining of ChAT in the whole-mount retina at P10 with (left) or without (right) DT treatment. Scale bar, 20 μm. Images were background-subtracted. (**C**) Number of SACs per unit area (1×10^4 μm^2). Each data point represents the averaged quantification from one retina (no inj: n = 8 retinas, 16.79 ± 0.74; PBS: n = 6 retinas, 14.17 ± 1.36; DT: n = 7 retinas, 2.98 ± 0.67; ***P = 0.0009, Kruskal-Wallis test; Tukey's post hoc test, no injection versus PBS P = 0.659, no injection versus DT ***$P = 7.405 \times 10^{-4}$, PBS versus DT *P = 0.028). (**D**) Frequency distributions of wave propagation directions

show that SAC-depleted retinas lack temporal-to-nasal propagation bias. Left to right, no injection (n = 8 hemispheres, total CV = 0.5167), PBS-injected (n = 10 hemispheres, total CV = 0.5475), and DT-injected (n = 7 hemispheres, total CV = 0.8373). (**E**) Proportion of wave propagation directions within 60° surrounding the dominant direction (no inj = 0.347 ± 0.014; PBS = 0.332 ± 0.027; DT = 0.146 ± 0.021; $^{**}P$ = 0.0011, Kruskal-Wallis test; Tukey's post hoc test, no injection versus DT-injected $^{**}P$ = 0.0043, PBS injection versus DT-injected $^{**}P$ = 0.0024, no injection versus PBS-injected P = 1). (**F**) Left: FRMD7^{tm} mice received intraocular injections of AAV2/1-hSyn-GCaMP6s at P0. Middle right: FRMD7^{tm} mice lack temporal-to-nasal wave propagation bias as revealed by the frequency distribution of wave propagation directions in littermate controls (n = 11 hemispheres, total CV = 0.559) and in FRMD7^{tm} mice (n = 9 hemispheres, total CV = 0.9214) at P10. (**G**) Proportion of wave propagation directions within 60° surrounding the dominant direction (control, 0.353 ± 0.027; FRMD7^{tm}, 0.145 ± 0.010; $^{***}P = 1.971 \times 10^{-6}$, Wilcoxon rank sum test). Dashed black lines in (E) and (G) indicate the fraction in the dominant direction if wave propagation directions are random. (**H**) Schematic models of retinal circuits that generate temporal-to-nasal directional waves during stage 2 (left) and stage 3 (right). Left: Stage 2 retinal waves propagate via SAC release of acetylcholine (blue) onto other cells, wave directionality is mediated by asymmetric GABAergic inhibition (red) among the recurrent SAC network. Greater inhibition on the nasal SAC dendrite prevents temporal propagation of waves. Right: Stage 3 retinal waves propagate via spillover of glutamate (green) from bipolar cells (BCs) onto other BCs, wave directionality is mediated by asymmetric GABAergic inhibition among SACs, and their feedback onto BCs. Feedback from SACs onto BCs may also be relayed by other types of intermediate amacrine cells in the retina (*41*).

(*42*) and JamB-positive ganglion cells that lack strong asymmetric inhibitory input from starburst amacrine cells in the adult retina (*43*). If wave directionality arises at the synapse between starburst amacrine cells and direction-selective ganglion cells, which emerges around P8 (*44*, *45*), we should observe a dorsal-ventral propagation bias in Cdh6-positive ganglion cells and little propagation bias in JamB-positive ganglion cells at P10. However, waves in both JamB-positive and Cdh6-positive ganglion cells propagated in the temporal-to-nasal direction (fig. S9 and movie S6). These data demonstrate that retinal ganglion cells inherit biased propagating activity from upstream circuits in the retina, not from asymmetric inhibitory inputs from starburst amacrine cells onto direction-selective ganglion cells. Our results also suggest that starburst amacrine cells modulate wave directionality by providing inhibition onto other cell types involved in wave propagation, perhaps onto starburst amacrine cells themselves during stage 2 and directly onto bipolar cells or indirectly onto bipolar cells via other amacrine cells (*41*) during stage 3 (Fig. 3H). Further experiments are required to test these hypotheses.

Directional retinal waves enhance downstream visual function

To directly probe the role of directional waves in visual system development, we chronically manipulated the directionality of spontaneous retinal waves and measured the visual function of neurons in the superior colliculus at eye opening. We used two-photon imaging to record the activity of neurons expressing nucleus-targeted GCaMP6s in the superior colliculus of Emx1-Cre; Tra2β$^{f/f}$ mice (Fig. 4A). To specifically disrupt wave directionality, we performed intraocular injections of gabazine (or saline) every 24 hours from P7 to P12 (Fig. 4A). We collected cellular responses in the superficial layers (50 to 60 μm) at the center of the superior colliculus 2 to 4 days after the last gabazine treatment (at P14–P16) in awake head-fixed mice as they viewed drifting grating visual stimuli (Fig. 4A). Drifting gratings elicited responses from similar proportions of neurons in saline-treated and chronic gabazine–treated mice (fig. S10A). Cells that preferentially responded to certain directions or orientations were found in both groups (Fig. 4C and supplementary materials). For all responsive cells, we measured the strength of direction and orientation tuning with a global direction selectivity index (gDSI) and a global orientation selectivity index (gOSI). We observed a significant reduction overall in the direction selectivity of cells in chronic gabazine–treated mice relative to saline controls (Fig. 4D). In contrast, gabazine treatment had little effect on the orientation selectivity of neurons in the superior colliculus (fig. S11A).

To determine whether disruption of wave directionality affected the selectivity of neurons for specific stimulus directions, we divided the responsive cells into eight groups according to their preferred direction and compared the tuning strength in each group. We observed a significant change in the distribution of gDSI across directions in chronic gabazine–treated mice in comparison to saline-treated mice, but the strength of direction selectivity was not significantly altered in any single direction (Fig. 4E and fig. S10B). We next examined whether the disruption of wave directionality altered the proportion of direction-selective cells preferring different directions. To do so, we computed the proportion of direction-selective cells preferring each direction among all responding cells. Consistent with the overall reduction in the strength of direction selectivity, we observed that the overall proportion of direction-selective cells was also significantly reduced in chronic gabazine–treated mice relative to saline-treated mice (Fig. 4F). We also observed that the distribution of direction preference across the eight different directions was significantly altered in chronic gabazine–treated mice relative to saline-treated mice, with a significant reduction in the dorsal direction (Fig. 4G and fig. S10C). Finally, we examined whether orientation selectivity was impaired in an orientation-dependent way, even though gabazine treatment had no impact on overall orientation tuning. No difference between saline- and gabazine-treated groups was observed in the tuning strength for any orientation (fig. S11, A and B), and the proportion of orientation-selective cells preferring each orientation among all responding cells was not significantly different between saline and gabazine groups (fig. S11C).

Because the effects of gabazine had a restricted duration in vivo (fig. S13), the manipulation of wave directionality using chronic intraocular injections of gabazine was likely limited. To more consistently disrupt wave directionality, we examined the direction-selective responses of superior colliculus neurons in Emx1-Cre; Tra2β$^{f/f}$; FRMD7^{tm} mice, which lack a temporal-to-nasal wave directional bias, as described earlier (Fig. 3, F and G). Like our findings in chronic gabazine–treated mice, we observed a significant impact on direction selectivity, but not orientation selectivity, of neurons in the superior colliculus of FRMD7^{tm} mice at eye opening (P14–P16) relative to littermate controls (Fig. 4, J to M, and fig. S11, D to F). In particular, there was a significant decrease overall in the direction selectivity of responding neurons in FRMD7^{tm} mice relative to littermate controls (Fig. 4J) and a significant change in the distribution of gDSI across the eight directions, with significant reductions in the temporal quadrant of directions in retinal coordinates (Fig. 4K and fig. S10E). Like the results of chronic gabazine treatment, we also observed a significant reduction in the overall proportion of direction-selective neurons among all responding neurons in the superior colliculus of FRMD7^{tm} mice (Fig. 4L). When divided according to direction preference, we also observed a significant change in the distribution of direction preference in FRMD7^{tm} mice relative to control mice, with a significant reduction in the temporal quadrant (Fig. 4M and fig. S10F). Direction selectivity is reduced in temporal- and nasal-preferring direction-selective retinal ganglion cells in FMRD7^{tm} mice (*38*), which may have contributed to the changes observed here in the superior colliculus. However, although there was an overall reduction in both the tuning and proportion of direction-selective cells in the superior colliculus of FMRD7^{tm} mice, only cells preferring the temporal

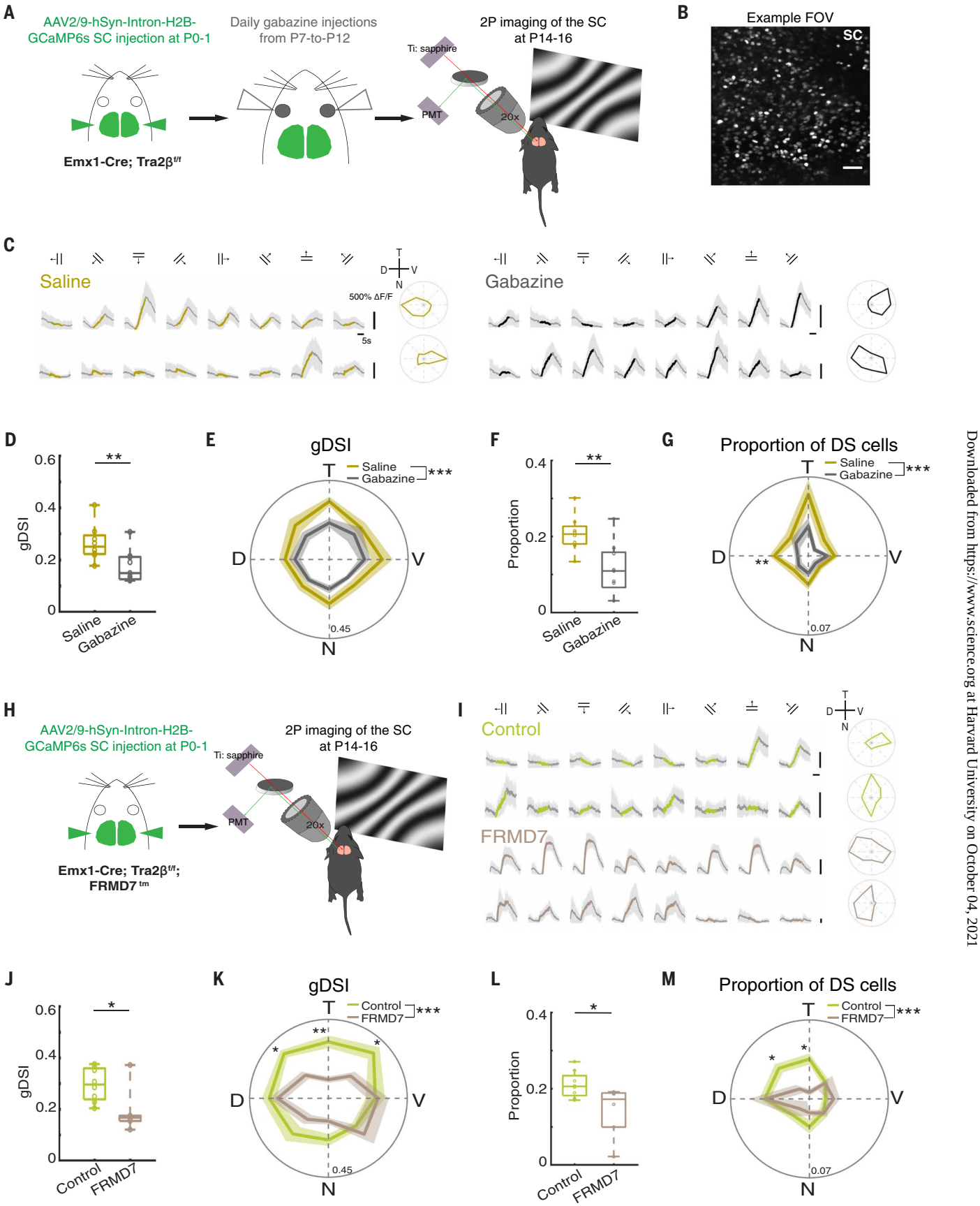

Fig. 4. Wave directionality instructs development of visual response properties. (**A**) AAV2/9-Syn-Intron-H2B-GCaMP6s was injected into both hemispheres of the SC in Emx1-Cre; Tra2β$^{f/f}$ mice at P0–P1. Mouse pups then received daily (chronic) intraocular injections of gabazine (200 μM) from P7 to P12. Two-photon imaging of SC neurons in the center of the left SC in response to visual stimuli presented to the right eye was performed in P14–P16 mice. (**B**) Example two-photon field of view in the SC ~50 μm from the surface. Scale bar, 50 μm. (**C**) Average fluorescence signal (ΔF/F ± SD) of individual neurons in the left SC of an example saline-treated P15 mouse (left) and an example chronic gabazine–treated P15 mouse (right) in response to 20 repetitions each of drifting gratings in eight directions. For each trial, gratings were static for 8 s, drifting for 8 s, and then static for another 8 s before switching to another direction. Solid lines, averaged ΔF/F signal where colored part indicates the ΔF/F during drifting grating period; gray shadow, SD of ΔF/F. Top, direction of drifting grating stimuli. The left most direction is nasal-to-temporal (backward-to-forward in visual space), the third from the left is ventral-to-dorsal (upward-to-downward in visual space). (Right) Polar plots of the averaged responses to each direction, with inset showing temporal (T), nasal (N), dorsal, (D) and ventral (V) directions in retinal coordinates. (**D**) Median gDSI of all responding cells in chronic gabazine–treated mice (n = 9) was significantly lower than in saline-treated mice (n = 8) (saline, 0.265 ± 0.025; gabazine, 0.175 ± 0.021; $^{**}P$ = 0.008, Wilcoxon rank sum test). (**E**) Polar plot showing the median gDSI of responding cells in saline- and gabazine-treated mice. Cells were divided into eight groups according to the directions for which they had the largest responses (see supplementary materials). The distribution of gDSI across directions was significantly altered in chronic gabazine–treated mice in comparison to saline-treated mice ($^{***}P = 2.724 \times 10^{-4}$, Mack-Skillings test; $P > 0.05$ for individual directions, Wilcoxon rank sum test with Benjamini-Hochberg false discovery rate adjustment). Solid line and shadow, mean ± SEM of median gDSI across all animals. Polar plot r range, [0, 0.45]. (**F**) The proportion of direction-selective (DS) cells (gDSI > 0.25) among all responding cells was significantly reduced in chronic gabazine–treated mice relative to saline-treated mice (saline = 0.208 ± 0.017, gabazine = 0.113 ± 0.023; $^{**}P$ = 0.008, Wilcoxon rank sum test). (**G**) The distribution of direction preference of DS cells among all responding cells was significantly altered in chronic gabazine–treated mice relative to saline-treated mice ($^{***}P = = 4.002 \times 10^{-6}$, Mack-Skillings test), with a significant reduction in the dorsal direction ($^{**}P$ = 0.005, Wilcoxon rank sum test with Benjamini-Hochberg false discovery rate adjustment). Solid line and shadow, mean ± SEM of proportions across all mice. Polar plot r range, [0, 0.07]. (**H**) Emx1-Cre; Tra2β$^{f/f}$; FRMD7^{tm} and littermate control mice received AAV2/9-Syn-Intron-H2B-GCaMP6s injections into the SC at P0–P1 and then visual response properties of SC neurons were measured using two-photon imaging of the center of left SC at P14–P16. (**I**) Average fluorescence signals (ΔF/F ± SD) of individual neurons in the left SC of an example littermate control P15 mouse (upper) and an example Emx1-Cre; Tra2β$^{f/f}$; FRMD7^{tm} P15 mouse (lower) in response to 20 repetitions of drifting gratings in each of eight directions. (**J**) The median gDSI of all responding cells was significantly reduced in FRMD7^{tm} mice (n = 6 animals) relative to controls (n = 8 animals) (control, 0.182 ± 0.035; FRMD7^{tm}, 0.144 ± 0.021; $^{*}P$ = 0.029, Wilcoxon rank sum test). (**K**) The distribution of gDSI across directions was significantly altered in FRMD7^{tm} mice relative to control mice ($^{***}P = 2.361 \times 10^{-13}$, Mack-Skillings test), with a significant reduction in the ventral-temporal ($^{*}P$ = 0.021), temporal ($^{**}P$ = 0.005), and dorsal-temporal ($^{*}P$ = 0.011) directions (Wilcoxon rank sum test with Benjamini-Hochberg false discovery rate adjustment). Solid line and shadow, mean ± SEM of median gDSI across all animals. Polar plot r range, [0, 0.45]. (**L**) The proportion of DS cells (gDSI > 0.25) among all responding cells was significantly reduced in FRMD7^{tm} mice relative to control mice (control = 0.211 ± 0.012, FRMD7^{tm} = 0.141 ± 0.028; $^{*}P$ = 0.029, Wilcoxon rank sum test). (**M**) The distribution of direction preference of DS cells among all responding cells was significantly altered in FRMD7^{tm} mice relative to control mice ($^{***}P = 2.569 \times 10^{-8}$, Mack-Skillings test), with a significant reduction in the temporal ($^{*}P$ = 0.011) and dorsal-temporal ($^{*}P$ = 0.019) directions (Wilcoxon rank sum test with Benjamini-Hochberg false discovery rate adjustment). Solid line and shadow, mean ± SEM of proportions across all animals. Polar plot r range, [0, 0.07].

and not the nasal quadrant of directions were significantly disrupted. This finding suggests that both the retina and colliculus may contribute to the disrupted development of direction-selective responses in superior colliculus neurons of FMRD7^{tm} mice.

To further examine whether impaired direction selectivity in the superior colliculus in chronic gabazine–treated and FRMD7^{tm} mice was a product of abnormal direction selectivity derived from the retina or alterations emerging in the superior colliculus, we treated mice with a single (acute) application of intraocular gabazine at eye opening immediately before imaging (fig. S14A). Gabazine application to the retina is known to disrupt direction-selective responses in retinal ganglion cells (*44*). In contrast to the effects of chronic gabazine well before eye opening (Fig. 4 and fig. S10), superior colliculus neurons in mice that received an acute gabazine injection showed no significant difference in the strength of direction selectivity or the proportion of direction-selective neurons (fig. S14, B to F), whereas direction-selective responses in the nasal but not the temporal quadrant were modestly degraded in the superior colliculus relative to controls (fig. S14, B to H). The differential effects of acute and chronic gabazine treatment on direction selectivity and the proportion of direction-selective cells suggests that disruptions in the development of circuits in the superior colliculus likely contribute to changes in the selectivity of superior colliculus neurons in chronic gabazine–treated mice and FRMD7^{tm} mice (Fig. 4 and fig. S10), although disruptions in the retina may also contribute. Overall, these results demonstrate that interfering with the directional bias of spontaneous retinal waves during development compromises the emergence of direction-selective responses in the superior colliculus at eye opening, highlighting the role of directional retinal waves in the emergence of functional response properties in mice.

Prior studies show that spontaneous retinal waves are necessary for the refinement of retinotopy in the superior colliculus (*11*, *12*, *20*, *21*). To investigate whether the impairment in direction selectivity in the superior colliculus can be explained by altered retinotopy, we quantified the refinement of retinotopy in the superior colliculus in mice with disrupted wave directionality. No difference was observed between the sizes of retinal ganglion cell arbors in the superior colliculus in FRMD7^{tm} mice and littermate controls (fig. S15). Furthermore, retinotopy measured at eye opening was similar between chronic gabazine–treated and chronic saline-treated mice (fig. S16). These data suggest that retinotopic refinement remained normal in mice with disrupted wave directionality, and exclude the possibility that retinotopic impairment contributes to the reduction of direction selectivity in the superior colliculus after the manipulation of wave directionality.

Discussion

Our data show that spontaneous retinal waves during development exhibit a distinct and strong propagation bias in the temporal-to-nasal direction during a transient window of development (P8 to P11) in mice. Directional waves mimic the translatory optic flow pattern that would be produced by an animal's own forward motion through space, a dominant optic flow pattern that is ethologically relevant after eye opening. Wave directionality during development is enforced by asymmetric inhibition through starburst amacrine cells mediated by $GABA_A$Rs, which is the same circuit element necessary for the computation of direction selectivity by retinal ganglion cells in the adult (*35*, *37*). Disrupting the directionality of spontaneous retinal waves compromises the emergence of direction-selective neurons in the superior colliculus at eye opening, causing

a general degradation in direction-selective responses and linking visual motion detection to retinal wave patterns during development.

The results of in vitro experiments suggest that starburst amacrine cells are responsible for the generation of stage 2 (P1–P9) retinal waves via their recurrent cholinergic neurotransmission (*22*, *32*–*34*, *46*). Here, we showed that starburst amacrine cells also enforce biased propagation of waves, even at P10–P11 when stage 3 waves are dependent on glutamatergic, not cholinergic, neurotransmission. Specifically, we found that asymmetric inhibitory outputs from starburst amacrine cells, which confer motion direction selectivity in direction-selective ganglion cells after the onset of vision (*35*–*37*), also mediate the temporal-to-nasal bias in wave directionality. This reveals an evolutionarily conserved link between the retinal circuitry responsible for biased wave propagation during development and the motion detection circuitry in mature retinas. There are also some differences between the developmental starburst amacrine cell–dependent wave propagation circuitry and the adult motion detection circuitry. Retinal waves in JamB-positive and Cdh6-positive ganglion cells, which prefer dorsal or ventral directions of motion in the adult retina, exhibit the same temporal-to-nasal wave propagation bias as the overall population of retinal ganglion cells during development. Because JamB-positive ganglion cells receive little inhibition from starburst amacrine cells (*43*), and because Cdh6-positive ganglion cells receive asymmetric inhibition from starburst amacrine cells along the dorsal-ventral axis (*42*), these results suggest that wave directionality is not generated by asymmetric inhibition from starburst amacrine cells onto direction-selective ganglion cells. Instead, direct or indirect asymmetric inhibition from starburst amacrine cells onto cells that are required for wave propagation—that is, starburst amacrine cells during stage 2 and bipolar cells during stage 3—mediates wave propagation bias.

Notably, the spatial geometry of the directional wave flow field resembles translatory optic flow from forward motion, which is the same optic flow pattern preferred by nasal-preferring direction-selective ganglion cells in the adult retina (*27*). This suggests that the asymmetric dendrites of starburst amacrine cells along the temporal-nasal axis that provide inhibition to nasal-preferring direction-selective ganglion cells—perhaps because they develop precociously or are more numerous (*27*)—may contribute the most to directional wave propagation. Further experiments are needed to examine this hypothesis.

Chronic blockade of $GABA_A$ transmission does not alter the development of direction selectivity in the retina, at least for a subset of direction-selective retinal ganglion cells for which this has been tested (*44*, *47*). In our experiments, we observed that blocking retinal direction selectivity with gabazine injections at eye opening, but leaving the directional waves intact earlier during development, resulted in little disruption in the direction selectivity of superior colliculus neurons. Moreover, $FRMD7^{tm}$ mice that lack a temporal-to-nasal wave directional bias exhibited a general disruption in the strength and proportion of direction-selective neurons in the superior colliculus, with a more specific effect on direction-selective cells preferring the temporal quadrant of directions. These results suggest that impaired direction selectivity of neurons in the superior colliculus after the disruption of wave directionality is not fully explained by disruptions in retinal ganglion cell directional selectivity, and likely involves miswiring between the retina and the superior colliculus or within the superior colliculus. Our data also suggest that direction selectivity in superior colliculus neurons at eye opening, unlike the adult (*48*), is not wholly dependent on direction-selective inputs from the retina. Further experiments are needed to determine the origin and mechanism underlying the computation of direction selectivity in the developing superior colliculus.

We used Emx1-Cre; $Tra2\beta^{f/f}$ (cortexless) mice because they have a fully accessible superior colliculus due to cortical agenesis. Although the absence of cortical feedback to the superior colliculus may compromise some visual functions (*26*, *49*), retinal waves in cortexless mice were similar to those in mice with an intact cortex, which suggests that waves were not altered in the absence of cortex during development. Previous studies also show that Emx1-Cre; $Tra2\beta^{f/f}$ mice have normal direction selectivity, orientation selectivity, and ON-OFF responses in the superior colliculus (*26*, *49*), indicating that the impairment of direction selectivity we observed in Emx1-Cre; $Tra2\beta^{f/f}$ mice after the disruption of wave directionality is not attributable to cortical agenesis.

Our experiments demonstrate that spontaneous retinal activity is self-structured to convey information essential for the development of visual response properties before the onset of visual experience. By simulating ethologically relevant features of the external environment, spontaneous retinal activity specifically and causally enhances higher-order visual function at eye opening. This is analogous to amphibian larvae, in which visual optic flow as the animal moves forward through space contributes to the development of retinotopy (*25*), as well as preplay in the developing mammalian hippocampus, where preconfigured sequences of neuronal firing foreshadow the development of hippocampal place cell memory function (*50*). Future experiments are necessary to determine the detailed mechanism by which wave directionality instructs the development of direction selectivity of neurons in the superior colliculus. Spontaneous retinal waves are transmitted through the entire developing visual system (*9*, *10*). Whether wave directionality contributes to the functional development of other downstream visual areas remains to be established.

Methods summary

All animal procedures followed the Yale Institutional Animal Care and Use Committee (IACUC), the US Department of Health and Human Services, and institution guidelines. Mouse pups received intraocular or intracollicular injections of virus encoding GCaMP6s at P0–P1 and were prepared with a craniotomy over the superior colliculus at later ages for wide-field calcium imaging of retinal ganglion cell axons in the superior colliculus or two-photon calcium imaging of superior colliculus neurons, respectively. Light stimulation or optogenetic stimulation of the retina was applied to initiate retinal waves in vivo. Retinal waves after acute intraocular injections of gabazine, TPMPA, or strychnine in mice at P10 were measured and analyzed to assess the role of inhibition in wave directionality. To ablate starburst amacrine cells, intraocular injections of diphtheria toxin (0.8 ng/μl in PBS) or PBS in littermate controls were performed daily from P5 to P7 in ChAT-Cre; iDTR mice. Daily gabazine (200 μM) injections (or saline injections in control mice) were performed from P7 to P12 to chronically disrupt wave directionality during development. Procedures for the experiments and data analyses are described in the supplementary materials.

REFERENCES AND NOTES

1. A. D. Huberman, M. B. Feller, B. Chapman, Mechanisms underlying development of visual maps and receptive fields. *Annu. Rev. Neurosci.* **31**, 479–509 (2008). doi: 10.1146/annurev.neuro.31.060407.125533; pmid: 18558864
2. T. A. Seabrook, T. J. Burbridge, M. C. Crair, A. D. Huberman, Architecture, Function, and Assembly of the Mouse Visual System. *Annu. Rev. Neurosci.* **40**, 499–538 (2017). doi: 10.1146/annurev-neuro-071714-033842; pmid: 28772103
3. L. E. White, D. Fitzpatrick, Vision and cortical map development. *Neuron* **56**, 327–338 (2007). doi: 10.1016/j.neuron.2007.10.011; pmid: 17964249
4. M. C. Crair, D. C. Gillespie, M. P. Stryker, The role of visual experience in the development of columns in cat visual cortex. *Science* **279**, 566–570 (1998). doi: 10.1126/science.279.5350.566; pmid: 9438851
5. N. L. Rochefort *et al.*, Development of direction selectivity in mouse cortical neurons. *Neuron* **71**, 425–432 (2011). doi: 10.1016/j.neuron.2011.06.013; pmid: 21835340
6. J. C. Horton, D. R. Hocking, An adult-like pattern of ocular dominance columns in striate cortex of newborn monkeys prior to visual experience. *J. Neurosci.* **16**, 1791–1807 (1996). doi: 10.1523/JNEUROSCI.16-05-01791.1996; pmid: 8774447
7. L. M. Chalupa, R. W. Rhoades, Directional selectivity in hamster superior colliculus is modified by strobe-rearing but not by dark-rearing. *Science* **199**, 998–1001 (1978). doi: 10.1126/science.622583; pmid: 622583
8. M. Weliky, L. C. Katz, Correlational structure of spontaneous neuronal activity in the developing lateral geniculate nucleus in vivo. *Science* **285**, 599–604 (1999). doi: 10.1126/science.285.5427.599; pmid: 10417392
9. J. B. Ackman, T. J. Burbridge, M. C. Crair, Retinal waves coordinate patterned activity throughout the developing visual

system. *Nature* **490**, 219–225 (2012). doi: 10.1038/nature11529; pmid: 23060192
10. A. Gribizis *et al*., Visual Cortex Gains Independence from Peripheral Drive before Eye Opening. *Neuron* **104**, 711–723.e3 (2019). doi: 10.1016/j.neuron.2019.08.015; pmid: 31561919
11. J. Cang, D. A. Feldheim, Developmental mechanisms of topographic map formation and alignment. *Annu. Rev. Neurosci.* **36**, 51–77 (2013). doi: 10.1146/annurev-neuro-062012-170341; pmid: 23642132
12. T. J. Burbridge *et al*., Visual circuit development requires patterned activity mediated by retinal acetylcholine receptors. *Neuron* **84**, 1049–1064 (2014). doi: 10.1016/j.neuron.2014.10.051; pmid: 25466916
13. H. P. Xu *et al*., Spatial pattern of spontaneous retinal waves instructs retinotopic map refinement more than activity frequency. *Dev. Neurobiol.* **75**, 621–640 (2015). doi: 10.1002/dneu.22288; pmid: 25787992
14. D. A. Butts, P. O. Kanold, C. J. Shatz, A burst-based "Hebbian" learning rule at retinogeniculate synapses links retinal waves to activity-dependent refinement. *PLOS Biol.* **5**, e61 (2007). doi: 10.1371/journal.pbio.0050061; pmid: 17341130
15. A. D. Huberman, C. M. Speer, B. Chapman, Spontaneous retinal activity mediates development of ocular dominance columns and binocular receptive fields in v1. *Neuron* **52**, 247–254 (2006). doi: 10.1016/j.neuron.2006.07.028; pmid: 17046688
16. C. L. Torborg, K. A. Hansen, M. B. Feller, High frequency, synchronized bursting drives eye-specific segregation of retinogeniculate projections. *Nat. Neurosci.* **8**, 72–78 (2005). doi: 10.1038/nn1376; pmid: 15608630
17. C. Pfeiffenberger, J. Yamada, D. A. Feldheim, Ephrin-As and patterned retinal activity act together in the development of topographic maps in the primary visual system. *J. Neurosci.* **26**, 12873–12884 (2006). doi: 10.1523/JNEUROSCI.3595-06.2006; pmid: 17167078
18. B. K. Stafford, A. Sher, A. M. Litke, D. A. Feldheim, Spatial-temporal patterns of retinal waves underlying activity-dependent refinement of retinofugal projections. *Neuron* **64**, 200–212 (2009). doi: 10.1016/j.neuron.2009.09.021; pmid: 19874788
19. B. Chapman, Necessity for afferent activity to maintain eye-specific segregation in ferret lateral geniculate nucleus. *Science* **287**, 2479–2482 (2000). doi: 10.1126/science.287.5462.2479; pmid: 10741966
20. J. Cang, L. Wang, M. P. Stryker, D. A. Feldheim, Roles of ephrin-as and structured activity in the development of functional maps in the superior colliculus. *J. Neurosci.* **28**, 11015–11023 (2008). doi: 10.1523/JNEUROSCI.2478-08.2008; pmid: 18945909
21. T. D. Mrsic-Flogel *et al*., Altered map of visual space in the superior colliculus of mice lacking early retinal waves. *J. Neurosci.* **25**, 6921–6928 (2005). doi: 10.1523/JNEUROSCI.1555-05.2005; pmid: 16033902
22. A. G. Blankenship, M. B. Feller, Mechanisms underlying spontaneous patterned activity in developing neural circuits. *Nat. Rev. Neurosci.* **11**, 18–29 (2010). doi: 10.1038/nrn2759; pmid: 19953103
23. A. Akrouh, D. Kerschensteiner, Intersecting circuits generate precisely patterned retinal waves. *Neuron* **79**, 322–334 (2013). doi: 10.1016/j.neuron.2013.05.012; pmid: 23830830
24. A. Maccione *et al*., Following the ontogeny of retinal waves: Pan-retinal recordings of population dynamics in the neonatal mouse. *J. Physiol.* **592**, 1545–1563 (2014). doi: 10.1113/jphysiol.2013.262840; pmid: 24366261
25. M. Hiramoto, H. T. Cline, Optic flow instructs retinotopic map formation through a spatial to temporal spatial transformation of visual information. *Proc. Natl. Acad. Sci. U.S.A.* **111**, E5105–E5113 (2014). doi: 10.1073/pnas.1416953111; pmid: 25385606
26. J. A. Shanks *et al*., Corticothalamic Axons Are Essential for Retinal Ganglion Cell Axon Targeting to the Mouse Dorsal Lateral Geniculate Nucleus. *J. Neurosci.* **36**, 5252–5263 (2016). doi: 10.1523/JNEUROSCI.4599-15.2016; pmid: 27170123
27. S. Sabbah *et al*., A retinal code for motion along the gravitational and body axes. *Nature* **546**, 492–497 (2017). doi: 10.1038/nature22818; pmid: 28607486
28. M. Chen, S. Weng, Q. Deng, Z. Xu, S. He, Physiological properties of direction-selective ganglion cells in early postnatal and adult mouse retina. *J. Physiol.* **587**, 819–828 (2009). doi: 10.1113/jphysiol.2008.161240; pmid: 19103682
29. N. Tian, D. R. Copenhagen, Visual stimulation is required for refinement of ON and OFF pathways in postnatal retina. *Neuron* **39**, 85–96 (2003). doi: 10.1016/S0896-6273(03)00389-1; pmid: 12848934
30. J. M. Rosa, R. D. Morrie, H. C. Baertsch, M. B. Feller, Contributions of Rod and Cone Pathways to Retinal Direction Selectivity Through Development. *J. Neurosci.* **36**, 9683–9695 (2016). doi: 10.1523/JNEUROSCI.3824-15.2016; pmid: 27629718
31. A. Tiriac, B. E. Smith, M. B. Feller, Light Prior to Eye Opening Promotes Retinal Waves and Eye-Specific Segregation. *Neuron* **100**, 1059–1065.e4 (2018). doi: 10.1016/j.neuron.2018.10.011; pmid: 30392793
32. J. Zheng, S. Lee, Z. J. Zhou, A transient network of intrinsically bursting starburst cells underlies the generation of retinal waves. *Nat. Neurosci.* **9**, 363–371 (2006). doi: 10.1038/nn1644; pmid: 16462736
33. K. J. Ford, A. L. Félix, M. B. Feller, Cellular mechanisms underlying spatiotemporal features of cholinergic retinal waves. *J. Neurosci.* **32**, 850–863 (2012). doi: 10.1523/JNEUROSCI.5309-12.2012; pmid: 22262883
34. H. P. Xu *et al*., Retinal Wave Patterns Are Governed by Mutual Excitation among Starburst Amacrine Cells and Drive the Refinement and Maintenance of Visual Circuits. *J. Neurosci.* **36**, 3871–3886 (2016). doi: 10.1523/JNEUROSCI.3549-15.2016; pmid: 27030771
35. S. I. Fried, T. A. Münch, F. S. Werblin, Mechanisms and circuitry underlying directional selectivity in the retina. *Nature* **420**, 411–414 (2002). doi: 10.1038/nature01179; pmid: 12459782
36. A. S. Mauss, A. Vlasits, A. Borst, M. Feller, Visual Circuits for Direction Selectivity. *Annu. Rev. Neurosci.* **40**, 211–230 (2017). doi: 10.1146/annurev-neuro-072116-031335; pmid: 28418757
37. W. R. Taylor, R. G. Smith, The role of starburst amacrine cells in visual signal processing. *Vis. Neurosci.* **29**, 73–81 (2012). doi: 10.1017/S0952523811000393; pmid: 22310373
38. K. Yonehara *et al*., Congenital Nystagmus Gene FRMD7 Is Necessary for Establishing a Neuronal Circuit Asymmetry for Direction Selectivity. *Neuron* **89**, 177–193 (2016). doi: 10.1016/j.neuron.2015.11.032; pmid: 26711119
39. D. Hillier *et al*., Causal evidence for retina-dependent and -independent visual motion computations in mouse cortex. *Nat. Neurosci.* **20**, 960–968 (2017). doi: 10.1038/nn.4566; pmid: 28530661
40. J. R. Sanes, R. H. Masland, The types of retinal ganglion cells: Current status and implications for neuronal classification. *Annu. Rev. Neurosci.* **38**, 221–246 (2015). doi: 10.1146/annurev-neuro-071714-034120; pmid: 25897874
41. A. Matsumoto *et al*., Synapse-specific direction selectivity in retinal bipolar cell axon terminals. bioRxiv https://www.biorxiv.org/content/10.1101/2020.10.12.335810v1 [preprint]. 12 October 2020.
42. J. N. Kay *et al*., Retinal ganglion cells with distinct directional preferences differ in molecular identity, structure, and central projections. *J. Neurosci.* **31**, 7753–7762 (2011). doi: 10.1523/JNEUROSCI.0907-11.2011; pmid: 21613488
43. I. J. Kim, Y. Zhang, M. Yamagata, M. Meister, J. R. Sanes, Molecular identification of a retinal cell type that responds to upward motion. *Nature* **452**, 478–482 (2008). doi: 10.1038/nature06739; pmid: 18368118
44. W. Wei, A. M. Hamby, K. Zhou, M. B. Feller, Development of asymmetric inhibition underlying direction selectivity in the retina. *Nature* **469**, 402–406 (2011). doi: 10.1038/nature09600; pmid: 21131947
45. K. Yonehara *et al*., Spatially asymmetric reorganization of inhibition establishes a motion-sensitive circuit. *Nature* **469**, 407–410 (2011). doi: 10.1038/nature09711; pmid: 21170022
46. M. B. Feller, D. P. Wellis, D. Stellwagen, F. S. Werblin, C. J. Shatz, Requirement for cholinergic synaptic transmission in the propagation of spontaneous retinal waves. *Science* **272**, 1182–1187 (1996). doi: 10.1126/science.272.5265.1182; pmid: 8638165
47. L. Sun, X. Han, S. He, Direction-selective circuitry in rat retina develops independently of GABAergic, cholinergic and action potential activity. *PLOS ONE* **6**, e19477 (2011). doi: 10.1371/journal.pone.0019477; pmid: 21573161
48. X. Shi *et al*., Retinal origin of direction selectivity in the superior colliculus. *Nat. Neurosci.* **20**, 550–558 (2017). doi: 10.1038/nn.4498; pmid: 28192394
49. K. H. Lee, A. Tran, Z. Turan, M. Meister, The sifting of visual information in the superior colliculus. *eLife* **9**, e50678 (2020). doi: 10.7554/eLife.50678; pmid: 32286224
50. U. Farooq, G. Dragoi, Emergence of preconfigured and plastic time-compressed sequences in early postnatal development. *Science* **363**, 168–173 (2019). doi: 10.1126/science.aav0502; pmid: 30630930

ACKNOWLEDGMENTS

We thank D. Clark, J. Demb, D. Lee, X. Papademetris, J. Zhou, and all members of the Crair lab for their helpful comments on this project; I.-J. Kim, X. Duan, and B. Roska for providing mouse lines; the Yale Vision Core for viral constructs; and especially Y. Zhang for help with mouse husbandry and genotyping. **Funding:** Supported by NIH grants R01EY015788, U01NS094358, P30EY026878, R01MH111424 (M.C.C.). M.C.C. also thanks the family of William Ziegler III for their support. **Author contributions:** X.G. and M.C.C. conceived and designed the study. X.G. performed and analyzed wide-field calcium imaging experiments. X.G. and K.Z. performed and analyzed two-photon calcium imaging experiments. A.G. helped with pharmacology experiments, A.S.H. helped with two-photon imaging experiments and A.M.S. helped with immunostaining experiments. X.G., K.Z., A.M.S., and M.C.C. analyzed and interpreted the results. X.G. and M.C.C. wrote the manuscript with input from all authors. **Competing interests:** Authors declare no competing interests. **Data and materials availability:** All data are available in the main text or the supplementary materials.

SUPPLEMENTARY MATERIALS

science.sciencemag.org/content/373/6553/eabd0830/suppl/DC1
Materials and Methods
Figs. S1 to S16
Table S1
Movies S1 to S6
References (*51*–*58*)

28 July 2020; accepted 26 May 2021
10.1126/science.abd0830

Retinal waves prime visual motion detection by simulating future optic flow

Xinxin GeKathy ZhangAlexandra GribizisAli S. HamodiAude Martinez SabinoMichael C. Crair

Science, 373 (6553), eabd0830.

Developing neurons practice for real life

As a mouse runs forward across the forest floor, the scenery that it passes flows backwards. Ge *et al*. show that the developing mouse retina practices in advance for what the eyes must later process as the mouse moves. Spontaneous waves of retinal activity flow in the same pattern as would be produced days later by actual movement through the environment. This patterned, spontaneous activity refines the responsiveness of cells in the brain's superior colliculus, which receives neural signals from the retina to process directional information. —PJH

Science, abd0830, this issue p. xxxx